Neuron 49, 877–887, March 16, 2006 ©2006 Elsevier Inc. DOI 10.1016/j.neuron.2006.02.018

Axons and Synaptic Boutons Are Highly Dynamic in Adult Visual Cortex

Dan D. Stettler,[1,3] Homare Yamahachi,[1] Wu Li,[1] Winfried Denk,[2] and Charles D. Gilbert[1,*]
[1] The Rockefeller University
New York, New York
[2] Max Planck Institute for Medical Research
JahnStrasse 29
D-69120 Heidelberg
Germany

Summary

While recent studies of synaptic stability in adult cerebral cortex have focused on dendrites, how much axons change is unknown. We have used advances in axon labeling by viruses and in vivo two-photon microscopy to investigate axon branching and bouton dynamics in primary visual cortex (V1) of adult Macaque monkeys. A nonreplicative adeno-associated virus bearing the gene for enhanced green fluorescent protein (AAV.EGFP) provided persistent labeling of axons, and a custom-designed two-photon microscope enabled repeated imaging of the intact brain over several weeks. We found that large-scale branching patterns were stable but that a subset of small branches associated with terminaux boutons, as well as a subset of en passant boutons, appeared and disappeared every week. Bouton losses and gains were both ∼7% of the total population per week, with no net change in the overall density. These results suggest ongoing processes of synaptogenesis and elimination in adult V1.

Introduction

Synaptic stability critically affects the function of brain circuits and could be necessary to maintain the integrity of neuronal functional properties. At the same time, alterations in cortical responses observed during perceptual learning or disruptions of sensory input might result from changes in connectivity that require synaptic pliability. Physiological plasticity could be mediated through synaptic changes at multiple spatial and temporal scales. Among other possibilities, synapses might be formed or eliminated through rearrangements of morphological structures such as dendritic spines and axon boutons. These rearrangements could occur either by small-scale alterations along stable neuronal processes or as the result of larger-scale changes in those processes. Studies in the cortex of adult mice suggest that spine morphology is mutable even under conditions where no training or disruption of input has occurred, though the degree of changeability is still debated (Grutzendler et al., 2002; Trachtenberg et al., 2002; Holtmaat et al., 2005; Zuo et al., 2005; at the end of the critical period: Majewska and Sur, 2003). It is unknown, however, whether axons and their boutons undergo morphological alterations in the normal adult cortex.

Recent advances have been made in the in vivo imaging of axons during development in mouse cortex (Portera-Cailliau et al., 2005) and in the midbrain of *Xenopus* (Cohen-Cory and Fraser, 1995; Alsina et al., 2001; Foa et al., 2001; Ruthazer et al., 2003; Hu et al., 2005), goldfish (during regeneration: Johnson et al., 1999), and zebrafish (Schmidt et al., 2000, 2004; Hua et al., 2005), as well as during development or adult plasticity in the spinal and peripheral circuitry of mouse, *Xenopus*, and zebrafish (Colman et al., 1997; Gan and Lichtman, 1998; Jontes et al., 2000; Buffelli et al., 2003; Kasthuri and Lichtman, 2003; Walsh and Lichtman, 2003; Bhatt et al., 2004; Bishop et al., 2004; Flanagan-Street et al., 2005; Javaherian and Cline, 2005; Kerschensteiner et al., 2005; Liu and Halloran, 2005; Schaefer et al., 2005). In the mouse, studies of axon development and dendritic stability have been carried out in animals that have been transgenically manipulated to express label in subpopulations of cells. We wished to study alterations in cortical circuitry in primates (Macaque monkeys), where transgenic approaches are impractical yet for which a large body of work has established conditions for plasticity of receptive field properties. In Macaque V1, for example, neuronal response properties can change as a result of training or disruption of input (Gilbert et al., 1990; Kaas et al., 1990; Gilbert and Wiesel, 1992; Chino et al., 1991, 1992; Heinen and Skavenski, 1991; Das and Gilbert, 1995; Crist et al., 2001; Schoups et al., 2001; Li et al., 2004). In vivo imaging of neuronal morphology in the Macaque has, however, faced the dual challenges of developing a means for long-term labeling of neurons and their processes with fluorescent probes and the need for a multi-photon microscope capable of accommodating large animals. These issues were addressed by using viral labeling of cortical neurons and developing a customized two-photon microscope (Denk et al., 1990).

Advances in the delivery of genetically encoded fluorophores have made it possible to completely label neurons and their processes in many species. A nonreplicative adenovirus (Ad) bearing the EGFP gene has been shown to provide effective labeling of adult cortical neurons without the need for histological processing (Stettler et al., 2002). While Ad.EGFP strongly and consistently labels somata, dendrites, and axons, it is of limited use for longitudinal studies because its labeling starts to decrease a couple of weeks after infection. Therefore, nonreplicative AAV.EGFP was tested as an alternative based upon its ability to drive long-term expression in adult neurons (Chamberlin et al., 1998; Bennett et al., 1999).

Two-photon imaging of neurons in the intact brain, originally demonstrated in rodents (Svoboda et al., 1997), is based on the confinement of excitation to a narrow focal plane and excitation at infrared wavelengths, which allow light penetration deep within cortical tissue (Denk and Svoboda, 1997). One limitation of two-photon

*Correspondence: gilbert@rockefeller.edu
[3] Present address: Howard Hughes Medical Institute, Columbia University, College of Physicians and Surgeons, 701 West 168th Street, New York, New York 10032.

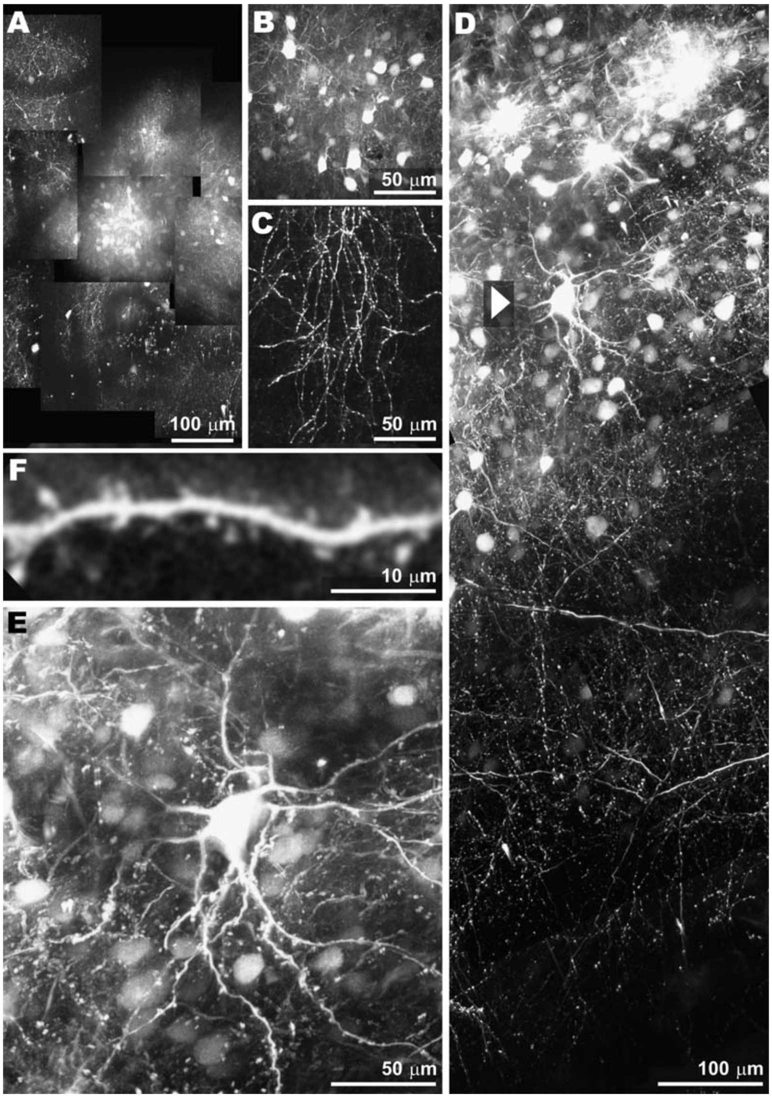

Figure 1. Strong and Persistent AAV.EGFP-Mediated Labeling of Macaque and Mouse V1 Neurons Imaged In Vivo with Two-Photon Microscopy

(A) Mouse V1 neurons labeled with AAV.EGFP and imaged in vivo. This montage was assembled from projections of z stacks acquired through a depth of 200 μm. Imaging was performed 4 weeks after injection. These and subsequent images of EGFP-labeled neurons have been filtered with a 2.0 pixel Gaussian filter to remove noise. These projections and others in this figure were calculated by maximum intensity.

(B) Injection site in mouse V1 imaged postmortem in a 50 μm section cut tangential to the cortical surface 1 year after injection of AAV.EGFP. The cell bodies remain strongly labeled and have normal morphology.

(C) AAV.EGFP-labeled mouse V1 axons 1 year after injection. The strongly labeled axons appear normal, with clearly identifiable boutons separated by narrower interbouton shafts.

(D) Macaque V1 cells labeled with AAV.EGFP and imaged in vivo. Strong labeling of cell bodies and processes is evident in this montage of projections from z stacks acquired through a depth of 300 μm in the intact cortex. Most labeled cell bodies lay within the densely labeled injection site at top, though some cell bodies also appear >100 μm away. The projections include data from every third z section.

(E) Cell indicated by the arrowhead in (D) at higher magnification. Note the spiny dendrites characteristic of excitatory neurons in cortex.

(F) Close-up of a spiny dendrite.

microscopy for larger animals is the need to move the imaged sample relative to the microscope's objective. To solve this problem, a microscope was custom-fitted with a second scanning head and a moveable objective to allow scanning over a large area while keeping the animal stationary. This arrangement, combined with a specially designed chamber that provides a window over V1, permitted repeated imaging of the same positions in Macaque V1. Using these techniques, we studied changes in the axons of adult Macaque visual cortical neurons that occur without the imposition of a systematic change in visual experience either through lesioning or training.

Results

Persistent Labeling and In Vivo Imaging

To test the labeling strength and persistence of the AAV.EGFP technique, high-titer injections were made into V1 of adult mice. Following the injections, EGFP labeling developed in neurons and glia within 3–4 weeks. Single time point in vivo two-photon microscopy of labeled cells and axons in mouse V1 established that labeling was visible in the intact brain (Figure 1A). The extent of cortical territory containing labeled cells depended on the injected volume, and bodies of labeled cells could be readily identified. In two cases, injected mice were examined after long survival periods, without interceding imaging sessions, to assess the persistence of the label. We found that cell bodies (Figure 1B) and processes, including axons (Figure 1C), remained well-labeled and appeared normal 1 year after viral injection.

AAV.EGFP injections in V1 of adult Macaques produced similar labeling (Figures 1D and 1F). In intact Macaque V1, EGFP-labeled somata and processes were discernible at high resolution to depths as far as 500 μm below the surface. Because superficial blood vessels cast shadows over imaged regions, somata and processes stretching over hundreds of micrometers were sporadically interrupted by linear dim regions. The virus produced strong (but not exclusive) labeling of pyramidal cells (Figure 1E) with well-filled spiny dendrites (Figure 1F) and axons (Figure 2). As in the mouse, strong labeling was maintained over long postinjection

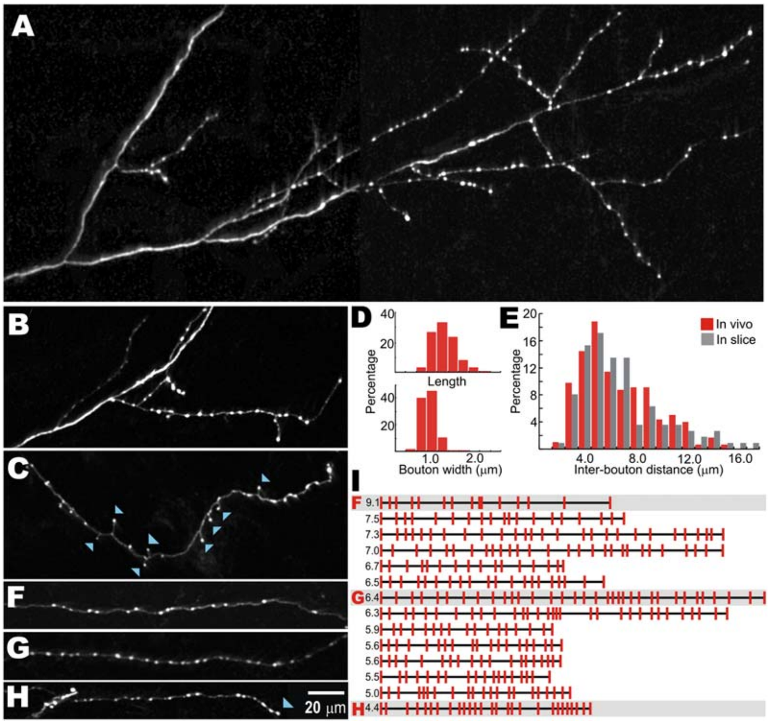

Figure 2. Similar Interbouton Distances of Axons Imaged In Vivo to Those Imaged in Postmortem Slices

(A and B) Axon arbors from Macaque V1 labeled with AAV.EGFP and imaged in vivo. The thicker portion of each axon in the lower left has little modulation of width but gives rise to multiple branches with distinguishable boutons. For much of these arbors, both en passant and terminaux boutons are unambiguously identifiable.

(C) For some axon segments, terminaux boutons (indicated with blue arrowheads) were also observed on the tips of small side branches.

(D) Distributions of in vivo bouton lengths (parallel to axon collateral) and widths (n = 291).

(E) Distributions of interbouton distances for axon segments imaged in vivo (red) and in postmortem slices (gray; n = 297 in vivo and 111 in slices).

(F–H) Sample images of axon segments with bouton positions schematically represented in (I).

(I) Schematic representations of bouton positions along axon segments are ordered from the highest average interbouton distance to the lowest, with the values (in micrometers) indicated at the left of each segment.

Scale bar applies to all images and (I).

periods in the Macaque. The longest postinjection period tested in a Macaque was 5 months.

Bouton Numbers In Vivo and Postmortem

Axons projecting from superficial (layers 1–3) neurons in Macaque V1 were labeled using AAV.EGFP and imaged in vivo through the superficial layers using two-photon microscopy (Figure 2). These axons were also imaged in the superficial layers. Boutons were identified as swellings along thinner axon shafts and measured 0.5–2.2 μm in length (mean = 1.2 ± 0.02 μm) and 0.5–1.5 μm in width (mean = 0.8 ± 0.01 μm; Figure 2D). Boutons were typically visible in two to three adjacent sections in acquired z stacks.

Some axon segments lacked boutons over most of their length but gave rise to distal branches with well-defined boutons (Figures 2A and 2B). Both terminaux and en passant boutons were observed, the former indicating the ends of axon branches (Figures 2B and 2C). Boutons terminating larger branches often were bigger than others. Interbouton distances on superficial layer Macaque V1 axons, imaged in vivo or in postmortem slices (Figure 2E), were on the average 6.3 ± 0.19 μm in vivo and 6.4 ± 0.38 μm postmortem in sections of perfused tissue. Individual axon segments exhibited a range of average interbouton distances (Figures 2F–2I).

Comparison of Axon Segments at Multiple Time Points

Locations in V1 containing axons were imaged at 1 week intervals. Imaging sites were matched using the blood vessel pattern by taking low-magnification reflected light pictures of the craniotomies and comparing them with montages of two-photon images obtained from the cortical surface during the first imaging session (Figure 3A). Imaged regions were between 1.5 and 3 mm from the AAV.EGFP injection sites and therefore contained labeled axons but not dendrites. These distances were also beyond the reach of dense local connections of excitatory and inhibitory cells. Moreover, while excitatory cells in deeper layers have horizontal connections that extend long distances in layers containing their somata, their projections to the superficial layers tend to have a more restricted lateral extent (Gilbert and Wiesel, 1979; Blasdel et al., 1985). Therefore, distance from the injection site, combined with distributions of boutonal characteristics consistent with a homogeneous population (Figure 2), indicate that the labeled axons were primarily the collaterals of long-range horizontal projections of superficial pyramidal cells.

Z stacks acquired through the superficial layers of V1 at 1 week intervals contained axon segments that could be identified and compared across time points (Figure 3B; imaging site indicated in Figure 3A). Regions containing many collaterals were separated by areas with fewer axons. Such modulation of density was expected due to the patchy character of the horizontal connections in Macaque V1 (Gilbert and Wiesel, 1979, 1983; Rockland and Lund, 1982).

Unlike the mouse, where dura (and even the thinned skull) are transparent enough for two-photon microscopy, the Macaque has a thick, opaque dura that must be removed before imaging. Removing the dura does not compromise the health of the cortex, which retains its blood supply and pia. However, after the dura has been removed, the surface of the cortex is subject to continuous growth of connective tissue. This tissue, while initially clear to the eye, later blocks two-photon imaging. For a few weeks after dura removal, the connective tissue can be stripped off without difficulty, but

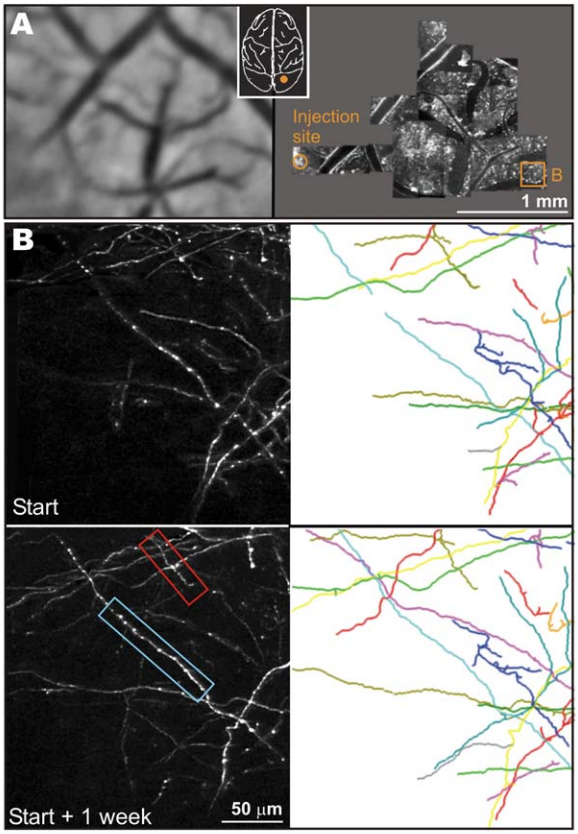

Figure 3. Axon Branching Assessed at Multiple Time Points

(A) Low-magnification reflected light image (left) of the surface vasculature over an exposed portion of V1 (position indicated in inset). The same vessel pattern can be seen in a montage (right) of superficial sections from two-photon z stacks from that region of V1. The AAV.EGFP injection site and location of axons seen in (B) are indicated. Scale bar, 1 mm.

(B) Projection of a field of axon segments imaged over a 100 μm depth 1 week apart. Before calculating the projections by maximum intensity, portions of individual z sections without axons were set to zero intensity to reduce background fluorescence. Most axons are visible at both time points. (Right) Individual axons were matched in the two data sets and traced in the z stacks (after processing with a 2 pixel Gaussian filter to reduce noise followed by brightness and contrast adjustment). Portions of some axons were not clearly visible during all imaging sessions due to growth of connective tissue on the surface of the cortex. Comparison of only those segments of axons that were clearly visible at multiple time points revealed no changes in the large-scale (>10 μm) branching patterns of axons. For a close-up of the axon segment in the blue box, see Figure 4, and for that in the red box, see Figure 6.

eventually it cannot be removed without damaging the cortex. Consequently, not all labeled axons were visible during every session. Reduction in axon brightness resulting from surface tissue could be distinguished from dimming or disappearance of axons themselves because it was matched by a reduction in background autofluorescence at the same depth and because, on occasions when the newly grown surface connective tissue could be successfully removed, the axons beneath became brighter. Because the presence of surface tissue is unlikely to be correlated with changes in connectivity in the underlying cortex, we chose axon segments for comparison across time points only if they appeared bright and their branching morphology was clearly discernible during all compared imaging sessions.

The same axons were identified at multiple time points and traced to determine their length. The dynamics of gross axon morphology were examined by counting how frequently new branches formed or existing branches disappeared and, when such changes were found, by how much the axon length changed. In total, 5.87 mm of axon in 16 locations from 2 animals was compared across two time points separated by 1 week. Axon branching remained largely stable with no branches longer than 11 μm appearing or disappearing (see below).

En Passant Bouton Dynamics

A subset of those axon segments that were compared over multiple time points had a morphology that was well enough defined to allow analysis of boutons. In all, 221 en passant boutons on 19 axon segments with a total length of 1.57 mm were compared in two animals. Frequent bouton additions and eliminations along collaterals were observed (Figures 4 and 5). These changes were independent of depth through the superficial layers. For each animal, the number of boutons added was similar to the number eliminated. The frequencies of these changes were similar between animals. In animal 1, which initially had 175 boutons on the tested segments, 11 (6.3%) of those boutons disappeared while 11 new en passant boutons appeared during 1 week. In animal 2, the numbers were as follows: 49 initial boutons, 4 (8.2%) appeared, 3 disappeared (6.1%). We only counted a bouton as having disappeared if the axon shaft at that location was discernible and the pattern of nearby boutons remained unchanged.

Some boutons were examined over a longer interval. Changes over a 2 week period (initial number = 50) included seven additions (14%) and six eliminations (12%) were about twice those observed over 1 week. Forty boutons were examined at three time points (start, start + 1 week, and start + 2 weeks). In this group, one bouton was added during the first week and eliminated during the second week (Figure 4).

Terminaux Bouton Dynamics

Large-scale changes in axon branching that involved additions or subtractions of axon collaterals longer than 11 μm were not observed. However, small side branches along axon shafts, nearly always bearing terminaux boutons, did appear (Figures 6A and 6B) and disappear (Figures 6A–6C). The set of axon segments examined for en passant bouton changes (total length 1.57 mm) possessed 22 side branches with terminaux boutons during the first imaging session. During a 1 week period, three side branches were subtracted and three new side branches having terminaux boutons were added. The entire set of axon segments examined for large-scale branching patterns (5.87 mm total) initially possessed 55 side branch terminaux boutons, with an average length of 4.2 ± 0.39 μm. During a 1 week interval, nine of these side branches were lost (with average length 3.1 ± 0.4 μm) and six new side branches bearing boutons were generated (4.3 ± 01.0 μm). These alterations were always less than 11 μm over a 1 week interval. The higher level of turnover exhibited by terminaux versus en passant boutons is

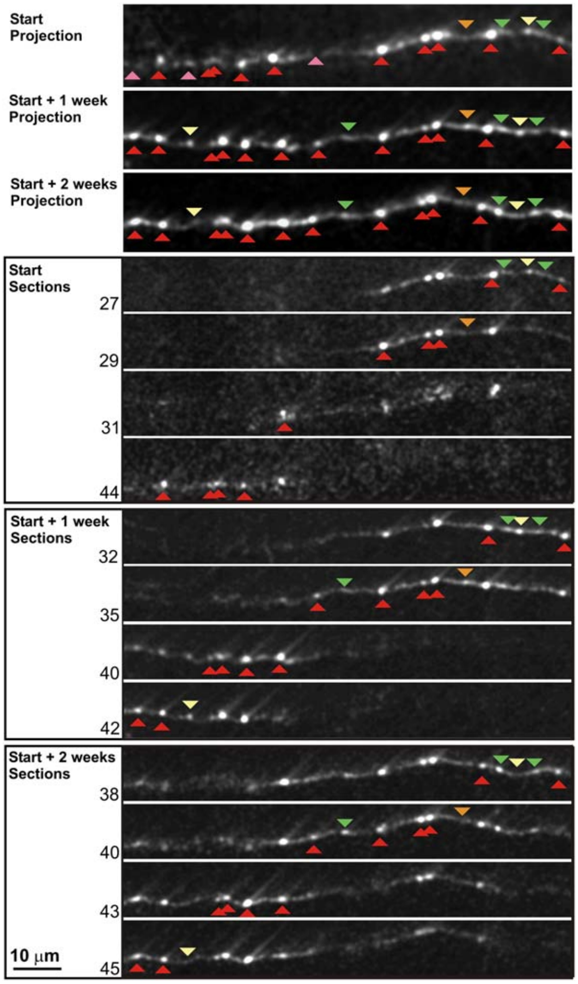

Figure 4. Boutons Added and Eliminated along Existing Axon Collaterals

At top, the same axon at three time points separated by 1 week intervals. The images are "cut-and-paste" projections in which the clearest representation of the axon at a given position was cut out of a single z section and compiled with representations of other positions from other z sections. This method reduces the distortions of local contrast produced by noise and autofluorescence in maximum intensity projections, but neither method conveys the full amount of information present in the z stacks, which were used for analyses of bouton appearances and disappearances. The image sets below are sample individual optical sections selected from the z stacks containing the axon. The right portion of this axon was bright at all three time points, but some boutons on the left portion could not be compared for the first time point due to dimness at that location during that imaging session. Red triangles mark boutons that did not change between time points. Yellow and green triangles mark disappeared and appeared boutons, respectively. The orange triangle marks a site where a bouton was present only during the second imaging session. Pink triangles mark sites that, during the first time point, could not be compared due to the dimness of the axon.

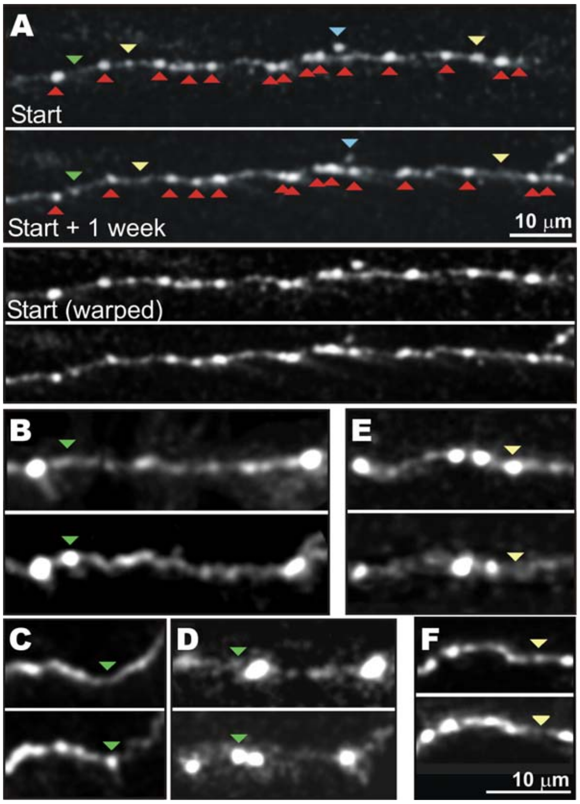

Figure 5. Additional Examples of En Passant Boutonal Dynamics

(A) An axon segment in which one new bouton was added and two boutons were eliminated over 1 week. (Color conventions as for Figure 4.) The top two panels depict cut-and-paste projections of the axon at two time points separated by 2 weeks. In the lower two panels, the projection of the "Start" time point has been stretched to aid the visual inspection of matching boutons.

(B–F) High-resolution views of three added (B–D) and two eliminated (E and F) boutons. Scale bar in (F) is correct for (B)–(F).

significant ($\chi^2 = 5.14$; df = 1; $p < 0.05$; losses and gains were pooled).

Most often, the changes in side branches involved the elimination or addition of the whole branch, including its bouton. In one case, however, an expansion from the tip of an existing side branch was observed that maintained the original bouton and added another, now terminaux, bouton. Also in one case, a terminaux bouton disappeared from a small branch containing a second, more proximal bouton that then became the terminaux bouton.

During one imaging session, a small branch that had appeared since the previous week's imaging session contracted over a period of 2 hr (Figure 7). The branch did not have a bouton at the start of the second session, so it is unclear whether it was a terminaux bouton caught in the process of disassembling or a filopodium that had never possessed a bouton. This lone observation is nevertheless intriguing given the higher turnover observed among the population of terminaux boutons compared to that of en passant boutons. The total rate of bouton turnover over a 1 week interval, including terminaux and en passant boutons, was therefore about 7%.

Discussion

The combination of persistent axon labeling, using AAV.EGFP, with in vivo two-photon imaging permits the comparison of selected axon segments longitudinally in time. We found that the morphology of long-range horizontal connections in intact V1 of adult Macaques was mutable on a short length scale (less than ~10 μm) on the time scale of 1 week. The overall rate

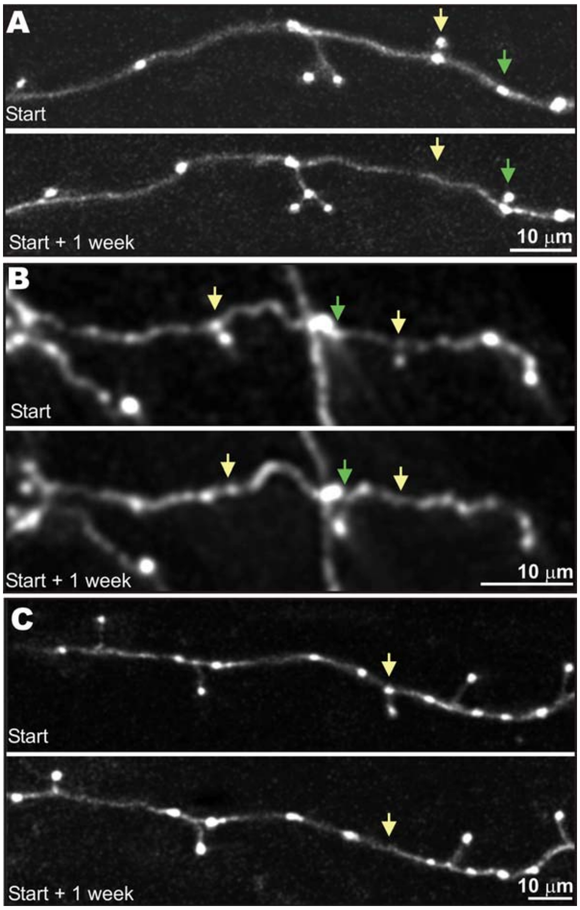

Figure 6. Extension and Contraction of Bouton-Bearing Side Branches

(A) Extension of a small side branch and contraction of another one, both with terminaux boutons, over 1 week.

(B) Axon segment with multiple side branch changes over 1 week.

(C) Contraction of a small side branch with a terminaux bouton.

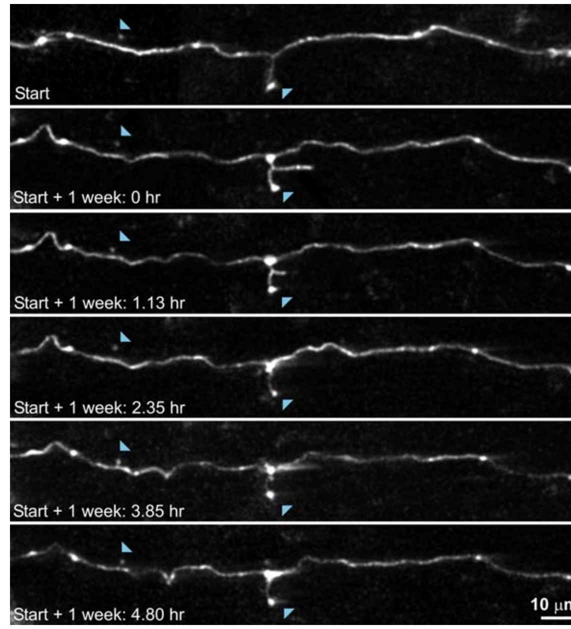

Figure 7. Fast Side Branch Dynamics

An axon segment during the initial imaging session (top) and then at multiple time points during the second session 1 week later. All images are projections. Note the small side branch (11 μm long) present at the beginning of the second session. This side branch contracted during the following 2 hr and did not reappear during the rest of the session. Most other features of the segment, including two terminaux boutons (blue arrowheads), remained unchanged.

of bouton turnover was about 7% per week, but the total number of boutons remained largely unchanged. A similar stability of large-scale axon branching patterns but pronounced mutability of terminaux and en passant boutons has recently been found for intracortical axons in barrel cortex of the mouse (De Paola et al., 2006 [this issue of *Neuron*]). These changes in axon morphology suggest that substantial genesis and elimination of synaptic connections occur in the adult cortex.

Bouton Designation and Prediction of Effective Synapses

The general agreement between the average interbouton distance seen in vivo, 6.3 μm, with that observed in postmortem cortical slices here and in other reports (Amir et al., 1993; cat: Anderson et al., 2003; mouse: Braitenberg and Schüz, 1998) indicates that our imaging technique had sufficient resolution to assess a representative population of boutons and that our criteria for identifying boutons matched those of earlier studies.

The appearance and disappearance of boutons observed in this study are very likely to reflect the formation and elimination of synapses. Neuronal morphological parameters have increasingly been found to relate to the existence and strength of synapses. Numerous studies of cortical axons have established that, when boutons are identified under light microscopy and subsequently examined with electron microscopy, nearly every bouton has at least one synapse, and synapses on axonal shafts between boutons are extremely rare (Somogyi, 1978; Peters and Proskauer, 1980; Winfield et al., 1981; Somogyi et al., 1982; Schuz and Munster, 1985; Kisvarday et al., 1986; Friedlander et al., 1991; McGuire et al., 1991; Peters et al., 1991; Anderson et al., 1998; Braitenberg and Schüz, 1998; Kincaid et al., 1998; Schikorski and Stevens, 1999; Anderson and Martin, 2001, 2005; Lubke et al., 2003; Silver et al., 2003). Due to the distance from the injection sites at which imaging was performed for this study, the imaged axons were predominantly the intrinsic long-range horizontal connections of superficial pyramidal cells (discussed below). For the intrinsic axons of pyramidal cells, all the boutons identified by light microscopy have been found by electron microscopy to form at least one synapse (Somogyi, 1978; Schuz and Munster, 1985; McGuire et al., 1991). Moreover, the lost and gained boutons observed in this study exhibited the same distribution of sizes as the static boutons (e.g., Figures 4 and 5). Accumulating evidence indicates that bouton size is positively related to active zone and postsynaptic density size (Pierce and Lewin, 1994; Harris and Sultan, 1995; Schikorski and Stevens, 1997, 1999). Therefore, the appearance and disappearance of boutons observed in vivo with two-photon imaging is likely to provide a reliable measure for cortical plasticity.

Bouton Dynamics in Adult Cortex

Depending on whether the population of boutons is homogeneous or not, the amount of bouton turnover (7% per week) has different implications for the stability of the synaptic connection network. If all boutons have the same replacement probability per unit time, synaptic connectivity would become largely remodeled after about 14 weeks. Alternatively, there may be a subpopulation of connections that are highly dynamic, with the rest remaining stable. The doubling of the total turnover observed with a doubling of the interval from 1 to 2 weeks is consistent with a uniform probability. However, so far only a limited number of boutons have been imaged at longer periods and more than two time points. Additional observations over longer periods and multiple time points will be necessary to resolve this issue conclusively.

For the current study, no systematic learning regimen or input disruption was used. The bouton turnover observed might nevertheless represent specific changes that were dependent on the animals' experience over the course of the experiment. An alternative possibility is that cortical circuitry turns over independent of experience, with bouton losses and gains occurring as independent stochastic processes. In either case, the correspondence between rates of bouton addition and elimination suggests regulation of total bouton number in cortical circuits. Addition and subtraction rates for presynaptic terminals in hippocampal slices have also recently been found to be equal (De Paola et al., 2003).

Besides addition and elimination of boutons along existing axon collaterals, a subset of axons showed the extension and contraction of small side branches ending in terminaux boutons. The dynamic rearrangement of such branches, which could occur within hours (Figure 7), expands the spatial range within which axons can choose their targets (Chklovskii et al., 2004). Similarly, fast changes in small-scale axon morphology have been observed in the intact mouse cortex (Dittgen et al., 2004).

The adult axon dynamics described here complement findings for dendrites in mouse cortex in vivo (Hering and Sheng, 2001; Chklovskii et al., 2004; Grutzendler et al., 2002; Trachtenberg et al., 2002; Majewska and Sur, 2003; Yuste and Bonhoeffer, 2004; Holtmaat et al., 2005; Zuo et al., 2005), which show that the branching of cortical pyramidal cell dendrites remains stable in the adult. Similar stability, characterized by only low rates of small expansions and contractions under ordinary circumstances, is seen in the dendritic branching of mitral and tufted cells of the olfactory bulb (Mizrahi and Katz, 2003). In contrast to this branching stability, spine formation and elimination have been seen in cortical dendrites. Spines apparently fall into at least two stability categories: those that persist for months and those that change over the course of days and weeks, with the distribution between these categories being disputed (Grutzendler et al., 2002; Trachtenberg et al., 2002; Holtmaat et al., 2005; Zuo et al., 2005). The rate of spine turnover in the somatosensory cortex can be altered by whisker trimming (Trachtenberg et al., 2002).

While the vast majority, if not all, of presynaptic sites in cortex involve boutons, spines are located only on the dendrites of the 80% of cortical neurons that are excitatory. Moreover, excitatory neurons receive synaptic input onto their dendritic shafts in addition to their spines (e.g., McGuire et al., 1991). Therefore, we cannot be sure whether or not an added or subtracted bouton corresponded to a synapse onto a spine. Regardless of the exact relationship between changing dendritic spines and boutons, the dynamic nature of axons in adult cortex demonstrated here argues against the notion that changes in connectivity are mediated only by postsynaptic structures, such as spines, choosing among static presynaptic partners.

Earlier studies in other systems employing in vivo imaging and less direct techniques demonstrate that axon stability is highly dependent upon the circuit in which an axon is embedded and the history of that circuit. During development, certainly, axons are universally dynamic and exhibit not only tremendous growth but also retraction or degeneration (Cohen-Cory and Fraser, 1995; Colman et al., 1997; Gan and Lichtman, 1998; Ruthazer et al., 2003; Walsh and Lichtman, 2003; Bishop et al., 2004; Hu et al., 2005; Javaherian and Cline, 2005; Jontes et al., 2000; Alsina et al., 2001; Buffelli et al., 2003; Kasthuri and Lichtman, 2003; Portera-Cailliau et al., 2005). Extensive axon regeneration in adults is observed after injury in the peripheral nervous system (recent in vivo imaging in the mouse: Nguyen et al., 2002; Pan et al., 2003) or, in nonmammalian vertebrates, in the central nervous system (e.g., Johnson et al., 1999; Bhatt et al., 2004). In V1, both thalamocortical axons and long-range horizontal connections go through processes of elimination and elaboration during development (Hubel et al., 1977; Callaway and Katz, 1990; Antonini and Stryker, 1993), by which they assume the large-scale organization that they maintain throughout adulthood under ordinary circumstances. This stability of axonal branching in the adult is supported by the current study. However, postmortem studies indicate that axon branching can occur in the neocortex of adult mammals following peripheral damage (discussed in the next section: Darian-Smith and Gilbert, 1994; Florence et al., 1998). One interesting theme that has emerged from studies both during development and in the adult is that competition plays an important role in determining axonal input to postsynaptic cells. Beyond the issue of stability of axonal branching, when one examines axons at the spatial scale of boutons as we do here (which has been relatively less well-studied), we do observe dynamics in the absence of explicit experimental intervention. Even so, it appears that some types of axons in the periphery, including motor nerve terminals innervating the neuromuscular junction (Lichtman et al., 1987; Balice-Gordon and Lichtman, 1990) and preganglionic terminals in the submandibular ganglion (Gan et al., 2003), are very stable in the adult mouse, with very few contacts being added or eliminated. The greater boutonal turnover observed here in the long-range horizontal connections of neocortex is intriguing considering recent findings showing experience-dependent changes in adult V1 associated with perceptual learning.

A Baseline Measure of Axon Dynamics

These experiments provide a baseline measure of axon and bouton dynamics in the absence of any systematic training or disruption of input. Because it is known that learning a given perceptual task leads to changes in the response properties of V1 neurons (Crist et al., 2001; Schoups et al., 2001; Li et al., 2004), it is tempting to speculate that during learning bouton turnover in the axons involved is accelerated so as to effect functional changes that underlie the learning. This may be particularly the case for those tasks that involve lateral interactions between stimuli lying within and outside of the classical receptive field and would thus require the long-range horizontal connections (Gilbert and Wiesel, 1979; Rockland and Lund, 1982; Stettler et al., 2002) that our experimental protocol specifically targets. Because horizontal connections of a given pyramidal cell may connect with each of their target cells at only a single synapse (McGuire et al., 1991), the addition and elimination of a small number of horizontal connection boutons might entail significant qualitative alterations in their connectivity. This nonredundancy of horizontal connectivity is not observed in the vertical circuitry of V1, which comprises relatively focused connections between cells within individual columns.

While we did not observe changes in larger-scale axon branching patterns, such changes might be more likely to occur under circumstances where gross changes in the connectivity between loci in cortex are expected, such as during intense training or disruption of input. An example is when input to V1 is disrupted by retinal lesions, which silence feedforward activation in small cortical "scotomas" and which lead, over time, to a reorganization of the cortical topography (Gilbert et al., 1990; Kaas et al., 1990; Gilbert and Wiesel, 1992; Chino et al., 1991, 1992; Heinen and Skavenski, 1991; Das and Gilbert, 1995; Schmid et al., 1996; Calford et al., 2000; but see Smirnakis et al., 2005). Postmortem analysis several months after lesioning reveals that long-range horizontal connections projecting to scotomas from surrounding cortex are much denser than connections to non-scotoma V1. Sprouting of horizontal connections extending into scotomas might explain how cells located there, initially silent after being deprived of their retinal input, acquire responses to the retinal input of surrounding regions of V1 (Darian-Smith and Gilbert, 1994; Arckens et al., 2000; Calford et al., 2003). Similar increases in horizontal connection density are found in somatosensory cortex after disruption of input, where functional reorganization is also observed (Merzenich et al., 1983; Calford and Tweedale, 1988; Pons et al., 1991; Florence et al., 1998).

The rate of bouton turnover found in this study (7% per week), even in the absence of imposed learning or retinal lesions, indicates that synapses are added and removed completely, i.e., that connection plasticity can involve more than changes in the effectiveness of existing synapses. The turnover rate is surprisingly large, particularly if one considers the implications such a rate would have, if sustained and homogeneous over all boutons, for maintaining basic functional properties. If the total population of synapses is labile, functional stability could still be maintained by the directed formation of new connections that recapitulate the existing functional maps. Alternatively, it is possible that turnover involves only a particularly labile subset of synapses, which would then be responsible for perceptual learning while the stable remainder mediates basic perceptual properties. Further work is needed to resolve this issue because the limited data at longer intervals presented here cannot strongly point to either possibility. Beyond the cortex in the normal adult, this issue is also relevant for how new neurons make appropriate connections in areas that undergo adult neurogenesis, such as mammalian hippocampus or in the bird song system, or when neural stem cells are introduced therapeutically to restore function in compromised brain areas.

Experimental Procedures

Animal Preparation and Viral Injections

All AAV.EGFP injections and two-photon imaging sessions were carried out in anesthetized *Macaca fascicularis* monkeys and mice in accordance with institutional and federal guidelines for the treatment of animals. Under nembutal anesthesia and with monitoring of heart rate and breathing, an adult Macaque was secured in a stereotactic apparatus. Following scalp retraction, a small (2 mm × 5 mm) hole was drilled through the skull overlying V1, and an incision was made in the dura. Aliquots of high-titer preparations of AAV.EGFP (80 nl containing 1.6×10^9 viral particles; capsid serotype 1) were pressured injected through glass micropipettes into superficial V1. Following viral injection, the scalp was sutured and the animal returned to its cage where it remained until imaging began at least 3 weeks later.

AAV.EGFP is a nonreplicative adeno-associated virus, the genes of which have been replaced by the gene encoding EGFP under control of the cytomegalovirus enhancer-promoter. AAV.EGFP vectors with three different capsid serotypes (1, 2, and 5) were tested. All imaged cells presented here were labeled with AAV.EGFP having a serotype 1 capsid. The virus was provided by Dr. Jean Bennett of the University of Pennsylvania and prepared as previously described (Xiao et al., 1999; Surace et al., 2003). The vectors were produced by transfection of 293 cells with three plasmids encoding (1) an EGFP expression cassette bearing the AAV serotype 2 inverted terminal repeats, (2) the AAV rep and cap genes, and (3) adenoviral helper function genes. The virus was subsequently purified through three successive centrifugations in CsCl gradients and titred using real-time PCR. AAV.EGFP is designed to minimize damage to infected cells caused by viral function or an induced immune response. The only native viral sequences present in the vector's DNA payload are the inverted terminal repeats necessary for packaging of the DNA in the viral capsid. Lack of damage is evidenced by the consistently normal morphology (including axons; see Figures 1A–1C for a 1 year interval) and density of labeled cells independent of time elapsed since the infection.

At the start of the first imaging session, the animal was fitted with a head-post. A custom-designed steel chamber that provided access for a microscope objective and that could be sealed between sessions was then fixed into place around the craniotomy using dental acrylic, and a larger (5–10 mm diameter) craniotomy was made surrounding the injection site. The dura was opened and retracted to expose an area of cortex ~6 mm in diameter. A quartz coverslip was then glued with surgical cyanoacrylate onto the edges of the opened dura. To maintain the clarity of the imaging window, the interior of the chamber was cleaned at the start of each imaging session and every 2–3 days otherwise. Animals were trained to sit in a restraint chair with their heads fixed so that the chamber could be cleaned on a regular basis between imaging sessions. Cleaning included the stripping of connective tissue that quickly began to cover the pia within the craniotomy.

In Vivo Imaging

Two-photon imaging was performed using a Leica (Heidelberg, Germany) TCS Sp2 confocal microscope that was custom fitted with a moveable scanning head (W.D. et al., unpublished data). The head was fastened to a frame extending from the side of the standard scan unit (from which it received its excitation path) and could be moved in three dimensions using a Sutter (Novato, CA) MP-285-3Z micromanipulator and also rotated around one axis. This modification freed up the space surrounding the objective to provide easier placement with respect to the Macaque's skull chamber. Two-photon excitation (930 nm) was provided by a Ti-sapphire laser pumped by a 10 W frequency-doubled Nd:Vandate Laser (Tsunami/ Millenia system, Spectra Physics, Mountain View, CA).

During the first session, imaging began at the injection site. Subsequently, nearby regions of cortex containing EGFP-labeled axons were identified and targeted for imaging on multiple occasions. Locating targeted regions within the chamber involved several steps. First, the identical pial vascular pattern could be seen in low-magnification images of the whole craniotomy and the higher-magnification superficial sections in two-photon z stacks. Next, a microscopic grid affixed to a special chamber insert was placed in the chamber. The grid could be navigated with the microscope under reflected light more easily than the blood vessels and allowed placement of the objective with <100 μm resolution. After identifying a landmark in the vascular pattern where axons had previously been imaged, the objective could be directed to that spot under reflected light using the overlying grid.

Imaging was performed with a 40× water-immersion objective (Nikon FLUOR 40X/0.08W DIC M) which gave a 250 μm field of view. Scanning was done at a resolution (0.24 μm per pixel) sufficient to see fine axons and boutons. Stacks of optical sections were acquired at 1 μm z intervals. Despite the fastening of a coverslip over the exposed cortex to reduce movement, brain movement on the order of one to a few micrometers in all three dimensions sometimes occurred. Collected z sections, therefore, were not always evenly spaced with regard to the tissue. The optical axis used for imaging was always perpendicular to the cortical surface, and any variation of imaging angle was likely to be within a few degrees. (It should also be noted that some specimen-orientation artifacts, if they exist, would not affect the main findings of the paper—complete loss or gain of en passant and terminaux boutons—because these changes are apparent regardless of the imaging angle.) To reconstruct axon projection zones over a larger area, we developed software to tile together numerous z stacks. Imaging sessions of several hours provided imaged areas ~2 mm across.

Several pieces of evidence indicate that the boutonal dynamics we observed were not the result of phototoxicity associated with imaging. First, morphological parameters such as bouton size and average distance between boutons did not change between consecutive imaging sessions. Second, the rates of change of boutons were the same for the 1 week and 2 week intervals. Finally, differences in the frequency of imaging sessions (twice versus three times over a 2 week period) did not appear to influence the bouton turnover.

Image Analysis

Axons and boutons were identified and traced or marked by hand in the raw z stacks of unprocessed two-photon images as well as stacks that had been processed with a Gaussian filter (1.5–2.0 pixel radius) to reduce noise. The examination of boutons involved multiple viewings of z stacks at different brightness and contrast levels as well as different zoom levels to verify their relationship with flanking axon shafts. En passant boutons were identified as swellings along thinner axon shafts, terminaux boutons as swellings at the ends of thinner axonal branches. These swellings were not always symmetrically placed with respect to the shafts' axes. Before analyzing the axons imaged at multiple time points, we analyzed well-labeled axons from single time point in vivo imaging sessions as well as postmortem in slices and found that our method produced interbouton distance distributions that were highly consistent across the two data sets (Figure 2) and that were similar to previously published findings (Amir et al., 1993; Anderson et al., 2003; Braitenberg and Schüz, 1998).

This analysis yielded a population of en passant boutons that ranged from 0.5 to 1.5 μm in width and 0.5 to 2.2 μm in length. Average dimensions across the population (length = 1.2 ± 0.02 μm and width = 0.8 ± 0.01 μm) were larger than those calculated based upon studies employing electron microscopy (McGuire et al., 1991; Peters et al., 1991; Ahmed et al., 1997; in mouse piriform layer 1B: Schikorski and Stevens, 1999), presumably because of blurring in the optical images, with a minor contribution possible due to shrinkage during tissue processing for EM. Differences in brightness between imaging sessions were the main reason that axon segments had to be disregarded for analysis. A thin but imaging-impermeable layer of tissue constantly regrew over the pia in the area where the dura, which in the Macaque is an opaque barrier, had been removed. Removal of the regrown tissue re-exposed many, but not all, imaging targets. Potential artifacts resulting from changes in brightness across time points were avoided by comparing only those axon segments that had clearly discernible morphology at all time points for which the boutons were compared.

For the longitudinal analyses, the correspondence of individual boutons between imaging sessions was examined in order to determine which boutons were stable over the full period and which boutons had appeared and disappeared within the period. A subset of axon segments was analyzed independently by two scorers. For each bouton, the scorers chose a confidence value of 1 to 4 to rate their certainty that the assignment was consistent with a set of agreed upon examples of boutons and non-boutons. The results of these analyses were similar overall and particularly so for the high-confidence assignments, which constituted the large majority of unchanged boutons and over half of the total number of reported losses and gains.

Acknowledgments

The authors would like to thank Justin McManus for statistical analysis and helpful discussions; Jean Bennett for providing the virus; and Priya Gogia, Travis Hartman, Keith Hazleton, and Tina Marney for invaluable technical assistance. This work was performed with support of NIH grant EY 012896 and with funding from the Max-Planck Society. W.D. possesses a patent on two-photon technology. The other authors declare that they have no financial conflicts of interest pertaining to the content of this paper.

Received: November 1, 2005
Revised: December 12, 2005
Accepted: February 7, 2006
Published: March 15, 2006

References

Ahmed, B., Anderson, J.C., Martin, K.A.C., and Nelson, J.C. (1997). Map of the synapses onto layer 4 basket cells of the primary visual cortex of the cat. J. Comp. Neurol. *380*, 230–242.

Alsina, B., Vu, T., and Cohen-Cory, S. (2001). Visualizing synapse formation in arborizing optic axons in vivo: dynamics and modulation by BDNF. Nat. Neurosci. *4*, 1093–1101.

Amir, Y., Harel, M., and Malach, R. (1993). Cortical hierarchy reflected in the organization of intrinsic connections in Macaque monkey visual cortex. J. Comp. Neurol. *334*, 19–46.

Anderson, J.C., and Martin, K.A.C. (2001). Does bouton morphology optimize axon length? Nat. Neurosci. *4*, 1166–1167.

Anderson, J.C., and Martin, K.A.C. (2005). Connection from cortical area V2 to V3A in macaque monkey. J. Comp. Neurol. *488*, 320–330.

Anderson, J.C., Binzegger, T., Martin, K.A.C., and Rockland, K.S. (1998). The connection from cortical area V1 to V5: a light and electron microscopic study. J. Neurosci. *18*, 10525–10540.

Anderson, J.C., Binzegger, T., Douglas, R.J., and Martin, K.A.C. (2003). Chance or design? Some specific considerations concerning synaptic boutons in cat visual cortex. J. Neurocytol. *31*, 211–229.

Antonini, A., and Stryker, M.P. (1993). Development of individual geniculocortical arbors in cat striate cortex and effects of binocular impulse blockade. J. Neurosci. *13*, 3549–3573.

Arckens, L., Schweigart, G., Qu, Y., Wouters, G., Pow, D.V., Vandesande, F., Eysel, U.T., and Orban, G.A. (2000). Cooperative changes in GABA, glutamate and activity levels: the missing link in cortical plasticity. Eur. J. Neurosci. *12*, 4222–4232.

Balice-Gordon, R.J., and Lichtman, J.W. (1990). In vivo visualization of the growth of pre- and postsynaptic elements of neuromuscular junctions in the mouse. J. Neurosci. *10*, 894–908.

Bennett, J., Maguire, A.M., Cideciyan, A.V., Schnell, M., Glover, E., Anand, V., Aleman, T.S., Chirmule, N., Gupta, A.R., Huang, Y., et al. (1999). Stable transgene expression in rod photoreceptors after recombinant adeno-associated virus-mediated gene transfer to monkey retina. Proc. Natl. Acad. Sci. USA *96*, 9920–9925.

Bhatt, D.H., Otto, S.J., Depoister, B., and Fetcho, J.R. (2004). Cyclic AMP-induced repair of zebrafish spinal circuits. Science *305*, 254–258.

Bishop, D.L., Misgeld, T., Walsh, M.K., Gan, W.-B., and Lichtman, J.W. (2004). Axon branch removal at developing synapses by axosome shedding. Neuron *44*, 651–661.

Blasdel, G.G., Lund, J.S., and Fitzpatrick, D. (1985). Intrinsic connections of macaque striate cortex: axonal projection of cells outside lamina 4C. J. Neurosci. *5*, 3350–3369.

Braitenberg, V., and Schüz, A. (1998). Cortex: Statistics and Geometry of Neuronal Connectivity (Berlin: Springer).

Buffelli, M., Burgess, R.W., Feng, G., Lobe, C.G., Lichtman, J.W., and Sanes, J.R. (2003). Genetic evidence that relative synaptic efficacy biases the outcome of synaptic competition. Nature *424*, 430–434.

Calford, M.B., and Tweedale, R. (1988). Immediate and chronic changes in responses of somatosensory cortex in adult flying-fox after digit amputation. Nature *332*, 446–448.

Calford, M.B., Wang, C., Taglianetti, V., Waleszczyk, W.J., Burke, W., and Dreher, B. (2000). Plasticity in adult cat visual cortex (area 17) following circumscribed monocular lesions of all retinal layers. J. Physiol. *524*, 587–602.

Calford, M.B., Wright, L.L., Metha, A.B., and Taglianetti, V. (2003). Topographic plasticity in primary visual cortex is mediated by local corticortical connections. J. Neurosci. *23*, 6434–6442.

Callaway, E.M., and Katz, L.C. (1990). Emergence and refinement of clustered horizontal connections in cat striate cortex. J. Neurosci. *10*, 1134–1153.

Chamberlin, N.L., Du, B., de Lacalle, S., and Saper, C.B. (1998). Recombinant adeno-associated virus vector: use for transgene expression and anterograde tract tracing in the CNS. Brain Res. *793*, 169–175.

Chino, Y.M., Smith, E.L., III, Wada, H., Ridder, W.L., III, Langston, A.L., and Lesher, G.A. (1991). Disruption of binocularly correlated input leads to deficits in spatial properties of striate cortical neurons in cats. J. Neurophysiol. *65*, 841–859.

Chino, Y.M., Kaas, J.H., Smith, E.L., Langston, A.L., and Cheng, H. (1992). Rapid reorganization of cortical maps in adult cats following restricted deafferentation in retina. Vision Res. *32*, 789–796.

Chklovskii, D.B., Mel, B.W., and Svoboda, K. (2004). Cortical rewiring and information storage. Nature *431*, 782–788.

Cohen-Cory, S., and Fraser, S.E. (1995). Effects of brain-derived neurotrophic factor on optic axon branching and remodeling in vivo. Nature *378*, 192–196.

Colman, M., Nabekura, J., and Lichtman, J.W. (1997). Alterations in synaptic strength preceding axon withdrawal. Science *275*, 356–361.

Crist, R.E., Li, W., and Gilbert, C.D. (2001). Learning to see: experience and attention in primary visual cortex. Nat. Neurosci. *4*, 519–525.

Darian-Smith, C., and Gilbert, C.D. (1994). Axonal sprouting accompanies functional reorganization in adult cat striate cortex. Nature *368*, 737–740.

Das, A., and Gilbert, C.D. (1995). Long-range horizontal connections and their role in cortical reorganization revealed by optical-recording of cat primary visual cortex. Nature *375*, 780–784.

Denk, W., and Svoboda, K. (1997). Photon upmanship: why multiphoton imaging is more than a gimmick. Neuron *18*, 351–357.

Denk, W., Strickler, J.H., and Webb, W.W. (1990). Two-photon laser scanning microscopy. Science *248*, 73–76.

De Paola, V., Arber, S., and Caroni, P. (2003). AMPA receptors regulate dynamic equilibrium of presynaptic terminals in mature hippocampal networks. Nat. Neurosci. *6*, 491–500.

De Paola, V., Holtmaat, A., Knott, G., Song, S., Wilbrecht, L., Caroni, P., and Svoboda, K. (2006). Cell type-specific structural plasticity of axonal branches and boutons in the adult neocortex. Neuron *49*, this issue, 861–875.

Dittgen, T., Nimmerjahn, A., Komai, S., Licznerski, P., Waters, J., Margrie, T.W., Helmchen, F., Denk, W., Brecht, W., and Osten, P. (2004). Lenti-virus-based genetic manipulations of cortical neurons and their optical and electrophysiological monitoring *in vivo*. Proc. Natl. Acad. Sci. USA *101*, 18206–18211.

Flanagan-Street, H., Fox, M.A., Meyer, D., and Sanes, J.R. (2005). Neuromuscular synapses can form in vivo by incorporation of initially aneural postsynaptic specializations. Development *132*, 4471–4481.

Florence, S.L., Taub, H.B., and Kaas, J.H. (1998). Large-scale sprouting of cortical connections after peripheral injury in adult Macaque monkeys. Science *282*, 1117–1121.

Foa, L., Rajan, I., Haas, K., Wu, G.-Y., Brakeman, P., Worley, P., and Cline, H. (2001). The scaffold protein, Homer1b/c, regulates axon pathfinding in the central nervous system *in vivo*. Nat. Neurosci. *4*, 499–506.

Friedlander, M.J., Martin, K.A.C., and Wassenhove-McCarthy, D. (1991). Effects of monocular visual deprivation on geniculocortical innervation of area 18 in cat. J. Neurosci. *11*, 3268–3288.

Gan, W.B., and Lichtman, J.W. (1998). Synaptic segregation at the developing neuromuscular junction. Science *282*, 1508–1511.

Gan, W.-B., Kwon, E., Feng, G., Sanes, J.R., and Lichtman, J.W. (2003). Synaptic dynamism measured over minutes to months: age-dependent decline in an autonomic ganglion. Nat. Neurosci. *6*, 956–960.

Gilbert, C.D., and Wiesel, T.N. (1979). Morphology and intracortical projections of functionally chacterized neurons in the cat visual cortex. Nature *280*, 120–125.

Gilbert, C.D., and Wiesel, T.N. (1983). Clustered intrinsic connections in cat visual cortex. J. Neurosci. *3*, 1116–1133.

Gilbert, C.D., and Wiesel, T.N. (1992). Receptive field dynamics in adult primary visual cortex. Nature *356*, 150–152.

Gilbert, C.D., Hirsch, J.A., and Wiesel, T.N. (1990). Lateral interactions in visual cortex. Cold Spring Harb. Symp. Quant. Biol. *55*, 663–677.

Grutzendler, J., Kasthuri, N., and Gan, W.B. (2002). Long-term dendritic spine stability in the adult cortex. Nature *420*, 812–816.

Harris, K.M., and Sultan, P. (1995). Variation in the number, location and size of synaptic vesicles provides an anatomical basis for the nonuniform probability of release at hippocampal CA1 synapses. Neuropharmacology *34*, 1387–1395.

Heinen, S.J., and Skavenski, A.A. (1991). Recovery of visual responses in foveal V1 neurons following bilateral foveal lesions in adult monkey. Exp. Brain Res. *83*, 670–674.

Hering, H., and Sheng, M. (2001). Dendritic spines: structure, dynamics and regulation. Nat. Rev. Neurosci. *2*, 880–888.

Holtmaat, A.J., Trachtenberg, J.T., Wilbrecht, L., Shepherd, G.M., Zhang, X., Knott, G.W., and Svoboda, K. (2005). Transient and persistent dendritic spines in the neocortex *in vivo*. Neuron *45*, 279–291.

Hu, B., Nikolakopoulou, A.M., and Cohen-Cory, S. (2005). BDNF stabilizes synapses and maintains the structural complexity of optic axons in vivo. Development *132*, 4285–4298.

Hua, J.Y., Smear, M.C., Baler, H., and Smith, S.J. (2005). Regulation of axon growth in vivo by activity-based competition. Nature *434*, 1022–1026.

Hubel, D.H., Wiesel, T.N., and LeVay, S. (1977). Plasticity of ocular dominance columns in monkey striate cortex. Philos. Trans. R. Soc. Lond. B Biol. Sci. *278*, 377–409.

Javaherian, A., and Cline, H.T. (2005). Coordinated motor neuron axon growth and neuromuscular synaptogenesis are promoted by CPG15 in vivo. Neuron *45*, 505–512.

Johnson, F.A., Dawson, A.J., and Meyer, R.L. (1999). Activity-dependent refinement in the goldfish retinotectal system is mediated by the dynamic regulation of processes withdrawal: an in vivo imaging study. J. Comp. Neurol. *406*, 548–562.

Jontes, J.D., Buchanan, J., and Smith, S.J. (2000). Growth cone and dendrite dynamics in zebrafish embryos: early events in synaptogenesis images in vivo. Nat. Neurosci. *3*, 231–237.

Kaas, J.H., Krubitzer, L.A., Chino, Y.M., Langston, A.L., Polley, E.H., and Blair, N. (1990). Reorganization of retinotopic cortical maps in adult mammals after lesions of the retina. Science *248*, 229–231.

Kasthuri, N., and Lichtman, J.W. (2003). The role of neuronal identity in synaptic competition. Nature *424*, 426–430.

Kerschensteiner, M., Schwab, M.E., Lichtman, J.W., and Misgeld, T. (2005). In vivo imaging of axonal degeneration and regeneration in the injured spinal cord. Nat. Med. *11*, 572–577.

Kincaid, A.E., Zheng, T., and Wilson, C.J. (1998). Connectivity and convergence of single corticostriatal axons. J. Neurosci. *18*, 4722–4731.

Kisvarday, Z.F., Martin, K.A.C., Freund, T.F., Magloczky, Z.S., Whitteridge, D., and Somogyi, P. (1986). Synaptic targets of HRP-filled layer III pyramidal cells in the cat striate cortex. Exp. Brain Res. *64*, 541–552.

Li, W., Piech, V., and Gilbert, C.D. (2004). Perceptual learning and top-down influences in primary visual cortex. Nat. Neurosci. *7*, 651–657.

Lichtman, J.W., Magrassi, L., and Purves, D. (1987). Visualization of neuromuscular junctions over periods of several months in living mice. J. Neurosci. *7*, 1215–1222.

Liu, Y., and Halloran, M.C. (2005). Central and peripheral axon branches from one neuron are guided differentially by semaphorin3D and transient axonal glycoprotein-1. J. Neurosci. *25*, 10556–10563.

Lubke, J., Roth, A., Feldmeyer, D., and Sakmann, B. (2003). Morphometric analysis of the columnar innervation domain of neurons connecting layer 4 and layer 2/3 of juvenile rat barrel cortex. Cereb. Cortex *13*, 1051–1063.

Majewska, A., and Sur, M. (2003). Motility of dendritic spines in visual cortex *in vivo*: changes during the critical period and effects of visual deprivation. Proc. Natl. Acad. Sci. USA *100*, 16024–16029.

McGuire, B.A., Gilbert, C.D., Rivlin, P.K., and Wiesel, T.N. (1991). Targets of horizontal connections in Macaque primary visual cortex. J. Comp. Neurol. *305*, 370–392.

Merzenich, M.M., Kaas, J.H., Wall, J., Nelson, R.J., Sur, M., and Felleman, D. (1983). Topographic reorganization of somatosensory cortical areas 3b and 1 in adult monkeys following restricted deafferentiation. Neuroscience *8*, 33–55.

Mizrahi, A., and Katz, L.C. (2003). Dendritic stability in the adult olfactory bulb. Nat. Neurosci. *6*, 1201–1207.

Nguyen, Q.T., Sanes, J.R., and Lichtman, J.W. (2002). Pre-existing pathways promote precise projection patterns. Nat. Neurosci. *5*, 861–867.

Pan, Y.A., Misgeld, T., Lichtman, J.W., and Sanes, J.R. (2003). Effects of neurotoxic and neuroprotective agents on peripheral nerve regeneration assayed by time-lapse imaging in vivo. J. Neurosci. *23*, 11479–11488.

Peters, A., and Proskauer, C.C. (1980). Synaptic relationships between a multipolar stellate cell and a pyramidal neuron in the rat visual cortex. A combined Golgi-electron microscope study. J. Neurocytol. *9*, 163–183.

Peters, A., Palay, S.L., and Webster, H. (1991). The Fine Structure of the Nervous System: Neurons and Their Supporting Cells (New York: Oxford).

Pierce, J.P., and Lewin, G.R. (1994). An ultrastructural size principal. Neuroscience *58*, 441–446.

Pons, T., Garraghty, P.E., Ommaya, A.K., Kaas, J.H., Taub, E., and Mishkin, M. (1991). Massive cortical reorganization after sensory deafferentiation in adult Macaques. Science *252*, 1857–1860.

Portera-Cailliau, C., Weimer, R.M., De Paola, V., Caroni, P., and Svoboda, K. (2005). Diverse modes of axon elaboration in the developing neocortex. PLoS Biol. *3*, e727 10.1371/journal.pbio.0030272.

Rockland, K., and Lund, J.S. (1982). Widespread periodic intrinsic connections in the tree shrew visual cortex. Science *215*, 1532–1534.

Ruthazer, E.S., Akerman, C.J., and Cline, H.T. (2003). Control of axon branch dynamics by correlated activity in vivo. Science *301*, 66–70.

Schaefer, A.M., Sanes, J.R., and Lichtman, J.W. (2005). A compensatory subpopulation of motor neurons in a mouse model of amyotrophic lateral sclerosis. J. Comp. Neurol. *490*, 209–219.

Schikorski, T., and Stevens, C.F. (1997). Quantitative ultrastructural analysis of hippocampal excitatory synapses. J. Neurosci. *17*, 5858–5867.

Schikorski, T., and Stevens, C.F. (1999). Quantitative fine-structural analysis of olfactory cortical synapses. Proc. Natl. Acad. Sci. USA *96*, 4107–4112.

Schmid, L.M., Rosa, M.G., Calford, M.B., and Ambler, J.S. (1996). Visuotopic reorganization in the primary visual cortex. Cereb. Cortex *6*, 388–405.

Schmidt, J.T., Buzzard, M., Borress, R., and Dhilon, S. (2000). MK801 increases retinotectal arbor size in developing zebrafish without affecting kinetics of branch elimination and addition. J. Neurobiol. *42*, 303–314.

Schmidt, J.T., Fleming, M.R., and Leu, B. (2004). Presynaptic protein kinase C controls maturation and branch dynamics of developing retinotectal arbors: possible role in activity-driven sharpening. J. Neurobiol. *58*, 328–340.

Schoups, A., Vogels, R., Qian, N., and Orban, G. (2001). Practising orientation identification improves orientation coding in V1 neurons. Nature *412*, 549–553.

Schuz, A., and Munster, A. (1985). Synaptic density on the axonal tree of a pyramidal cell in the cortex of the mouse. Neuroscience *15*, 33–39.

Silver, R.A., Lubke, J., Sakmann, B., and Feldmeyer, D. (2003). High-probability uniquantal transmission at excitatory synapses in barrel cortex. Science *302*, 1981–1984.

Smirnakis, S.M., Brewer, A.A., Schmid, M.C., Tolias, A.S., Schuz, A., Augath, M., Inhoffen, W., Wandell, B.A., and Logothetis, N.K. (2005). Lack of long-term cortical reorganization after Macaque retinal lesions. Nature *435*, 300–307.

Somogyi, P. (1978). The study of Golgi stained cells and of experimental degeneration under the electron microscope: a direct method for the identification in the visual cortex of three successive links in a neuron chain. Neuroscience *3*, 167–180.

Somogyi, P., Freund, T.F., and Cowey, A. (1982). The axon-axonic interneuron in the cerebral cortex of the rat, cat and monkey. Neuroscience *7*, 2577–2607.

Stettler, D.D., Das, A., Bennett, J., and Gilbert, C.D. (2002). Lateral connectivity and contextual interactions in Macaque primary visual cortex. Neuron *36*, 739–750.

Surace, E.M., Auricchio, A., Reich, S.J., Rex, T., Glover, E., Pineles, S., Tang, W., O'Connor, E., Lyubarsky, A., Savchenko, A., et al. (2003). Delivery of adeno-associated virus vectors to the fetal retina: impact of viral capsid proteins on retinal neuronal progenitor transduction. J. Virol. *77*, 7957–7963.

Svoboda, K., Denk, W., Kleinfeld, D., and Tank, D.W. (1997). *In vivo* dendritic calcium dynamics in neocortical pyramidal neurons. Nature *385*, 161–165.

Trachtenberg, J.T., Chen, B.E., Knott, G.W., Feng, G., Sanes, J.R., Welker, E., and Svoboda, K. (2002). Long-term *in vivo* imaging of experience-dependent synaptic plasticity in adult cortex. Nature *420*, 788–794.

Walsh, M.K., and Lichtman, J.W. (2003). In vivo time-lapse imaging of synaptic takeover associated with naturally occurring synapse elimination. Neuron *37*, 67–73.

Winfield, D.A., Brooke, N.L., Sloper, J.J., and Powell, T.P.S. (1981). A combined Golgi-electron microscopic study of the synapses made by the proximal axon and recurrent collaterals of a pyramidal cell in the somatic sensory cortex of the monkey. Neuroscience *6*, 1217–1230.

Xiao, W., Chirmule, N., Berta, S.C., McCullough, B., Gao, G., and Wilson, J.M. (1999). Gene therapy vectors based on adeno-associated virus type 1. J. Virol. *73*, 3994–4003.

Yuste, R., and Bonhoeffer, T. (2004). Genesis of dendritic spines: insights from ultrastructural and imaging studies. Nat. Rev. Neurosci. *5*, 24–34.

Zuo, Y., Lin, A., Chang, P., and Gan, W.B. (2005). Development of long-term dendritic spine stability in diverse regions of cerebral cortex. Neuron *46*, 181–189.